Journal of the Mechanics and Physics of Solids 58 (2010) 1011–1025

Contents lists available at ScienceDirect

Journal of the Mechanics and Physics of Solids

journal homepage: www.elsevier.com/locate/jmps

Plasticity of metal wires in torsion: Molecular dynamics and dislocation dynamics simulations

Christopher R. Weinberger *, Wei Cai

Department of Mechanical Engineering, Stanford University, CA 94305-4040, USA

ARTICLE INFO

Article history:
Received 19 February 2010
Received in revised form
16 April 2010
Accepted 24 April 2010

Keywords:
Microstructures
Dislocations
Grain boundaries

ABSTRACT

The orientation dependent plasticity in metal nanowires is investigated using molecular dynamics and dislocation dynamics simulations. Molecular dynamics simulations show that the orientation of single crystal metal wires controls the mechanisms of plastic deformation. For wires oriented along $\langle 1\,1\,0 \rangle$, dislocations nucleate along the axis of the wire, making the deformation homogeneous. These wires also maintain most of their strength after yield. In contrast, wires oriented along $\langle 1\,1\,1 \rangle$ and $\langle 1\,0\,0 \rangle$ directions deform through the formation of twist boundaries and tend not to recover when high angle twist boundaries are formed. The stability of the dislocation structures observed in molecular dynamics simulations are investigated using analytical and dislocation dynamics models.

1. Introduction

The plastic response of materials at the small scale is an area of great interest because as sample dimensions decrease, the material's mechanical response changes. The compression tests of micro- and nano-pillars has shown a dramatic increase in flow stress as a function of material size (Uchic et al., 2004; Greer et al., 2005). In addition, strain bursts become more prominent in small scale structures (Dimiduk et al., 2006; Csikor et al., 2007; Brinckmann et al., 2008) which may limit the ability of plastic metal-forming at the micro- and nano-scale (Csikor et al., 2007).

When materials are bent or twisted, they experience strain gradients which are known to alter the plastic response of the materials (Guzman et al., 1993; Fleck et al., 1994; Nix and Gao, 1998). This has lead to the development of strain gradient plasticity, which explains strengthening of materials at small scale through the interaction of statistically stored dislocations and geometrically necessary dislocations (Fleck and Hutchinson, 1993, 1997). Strain gradient plasticity theory has been successful in explaining strengthening observed in polycrystalline wires under torsion (Fleck et al., 1994). This naturally leads to the question of what happens when nanowires are twisted. Wires at this size are often single crystals, and there is very little experimental or numerical studies on plasticity of single crystal wires in torsion.

In this paper, we examine the plasticity of single crystal wires under torsion using both molecular dynamics (MD) and dislocation dynamics (DD) simulations. This will provide insight into how the deformation changes as a function of the wire's diameter. Since the wires are single crystals, we will study three high symmetry directions, $\langle 1\,1\,0 \rangle$, $\langle 1\,1\,1 \rangle$ and $\langle 1\,0\,0 \rangle$. The authors have already presented a discussion on the mechanisms of yield in these wires (Weinberger and Cai, 2010). In this work, we present a detailed look into the yield of the nanowires, boundary formation and stability.

* Corresponding author. Current Address: Sandia National Laboratories, P.O. Box 5800, MS1411, Albuquerque, NM 87185-1411, USA. Tel.: +1 505 284 0896.
E-mail addresses: crweinb@sandia.gov (C.R. Weinberger), caiwei@stanford.edu (W. Cai).

0022-5096/$ - see front matter © 2010 Elsevier Ltd. All rights reserved.
doi:10.1016/j.jmps.2010.04.010

Dislocation dynamics simulations will be presented in order to provide further understanding in the formation and dissolution of these structures.

2. Simulation methods

2.1. Molecular dynamics

To study the plasticity in metallic nanowires, the primary tool used here is molecular dynamics. To avoid end effects, torsional periodic boundary conditions (tPBC) are used in all of the simulations. The details of this method have been described previously by the authors (Cai et al., 2008) including discussions on how to measure torque. The loading is an applied affine twist enforced by the boundary conditions, the same way strain would be applied in MD simulations of uniaxial loading of nanowires. This leads to a constant twist rate and hence a constant surface shear strain rate simulation.

In order to fully understand the plasticity in nanowires, a large number of parameters are varied as part of this study. The orientations of the nanowires studied are three high symmetry directions, $\langle 1\,0\,0\rangle$, $\langle 1\,1\,0\rangle$ and $\langle 1\,1\,1\rangle$. Three diameters, 5, 7.5, and 10 nm, are used. The orientation and size of the nanowires are thought to provide the largest impact on plasticity in the nanowires. However, other effects will also be examined, including strain rates, aspect ratios, stacking fault energy, statistical variations, and surface defects.

The simulations are performed on two face-centered-cubic (FCC) metals, gold and aluminum, in order to capture the effect of stacking fault energies. The interatomic potential for gold is the EAM Foiles (Park and Zimmerman, 2005), which has a stacking fault energy of 31 mJ/m^2 and agrees very well with DFT calculations. The aluminum potential used is the EAM Mishin et al. (1999) with a stacking fault energy of 146 mJ/m^2. Since the stacking fault energy of gold is about five times smaller than aluminum, larger diameter gold wires are also investigated. The stacking fault energy is important for these simulations because the diameter of the wires studied approaches the equilibrium separation width between partial dislocations, governed by the stacking fault energy.

In order to compare different diameter wires, the nominal engineering surface shear strain rate is $4\times10^8\,\mathrm{s}^{-1}$ for all the simulations. This is accomplished by applying an incremental twist per unit length every 5 ps using a time step of 1 fs. We define the engineering shear strain rate as $\dot{\gamma}=\dot{\beta}r$, where $\dot{\beta}$ is the twist rate per unit length and r is the radius where the strain is evaluated. The surface engineering shear strain rate is found by evaluating r at the nanowire radius. Since the aspect ratio is held constant for all wires 10 nm and smaller, $\dot{\beta}$ and $\dot{\gamma}|_{r=R}$ are constants, where R is the radius of the nanowire. Thus the maximum applied twist is also a constant, at 0.8 radians or 46°.

In preparation for twisting, the wires are relaxed and equilibrated at 300 K. First, the nanowires are created from a bulk configuration and relaxed using conjugate gradient relaxation in order to alleviate axial stresses due to surface effects. Then, the wires are equilibrated at 300 K for 100 ps using a Nosé–Hoover thermostat and a Parrinello–Rahman barostat to eliminate stresses in the wire, reproducing a NσT ensemble. The equilibrium length of the nanowire is taken to be the average of the last half of the equilibration run.

The twisting simulations are then carried out using torsional periodic boundary conditions along the z-axis of the wire. In order to alleviate axial stress that develops during the simulation, caused by either elastic or plastic processes, the length of the wire is allowed to relax using the Parrinello–Rahman stress control (Parrinello and Rahman, 1981) in that direction. The twist is incremented, however, at fixed intervals simulating a constant twist rate experiment.

2.2. Dislocation dynamics

The dislocation dynamics simulations are performed using the ParaDiS code developed at Lawrence Livermore National Laboratory (Cai et al., 2004; Bulatov et al., 2004). The perfect dislocations are approximated as straight line segments. In order to simulate dislocation structures in a nanowire, the free surfaces must be accounted for. The authors use a modified version of the ParaDiS code for this purpose (Weinberger and Cai, 2007; Weinberger et al., 2009) which accurately computes the image stress and interactions with free surfaces.

The dislocation dynamics simulations are further modified to account for the applied torque. From elasticity theory, a torque applied to a circular shaft can be related to the shear stress as $\sigma_{z\theta}=\tau r/J$ where τ is the applied torque, r is radius of the point where the stress is evaluated and $J=(\pi/2)R^4$ is the polar moment of inertial of a circular shaft with radius R. The additional force on the dislocations can be evaluated by integrating over the segment lengths as discussed in Arsenlis et al. (2007). For simplicity, we use one point quadrature for evaluation of the nodal force contribution from the applied torque.

For simulations of dislocations in $\langle 1\,1\,0\rangle$ oriented wires, a two-dimensional dislocation dynamics code is used. The forces on the dislocations are computed by superimposing the fields of infinitely long screw dislocations in cylinders derived by Eshelby (1953) and Eshelby (1979). The contributions arise from forces due to the dislocations in an infinite medium, image forces required to make the surfaces traction free, and image torque forces required to make the rod torque free. Additional forces from an applied torque are also included. The dislocations are allowed to relax in the direction of the total Peach–Koehler forces.

3. Results

Fig. 1 shows torque twist curves for both gold and aluminum nanowires for all three orientations. From these results we can make a simple observation about strength. In general, aluminum is stronger than gold. This is in agreement with the difference in unstable stacking fault energies between the gold and aluminum potentials, which are 120 mJ/m^2 and 168 mJ/m^2 respectively.

For small angles, the torque is approximately linear with the applied twist, as predicted by linear elasticity. The relationship for isotropy is $\tau = J\mu\beta$ where τ is the torque, J is the polar moment of inertia and β is the twist per unit length. This can be used to approximate the torque twist relationship in the anisotropic case if we replace the isotropic shear modulus with the effective shear modulus of the plane in torsion. We computed the effective shear modulus by simply averaging over all the shear moduli on the plane under torsion. The resulting torque twist relationships are

$$\tau = \frac{1}{4}(C_{11}-C_{12}+2C_{44})J\beta \quad \langle 1\,1\,0\rangle$$

$$\tau = \frac{1}{3}(C_{11}-C_{12}+C_{44})J\beta \quad \langle 1\,1\,1\rangle$$

$$\tau = C_{44}J\beta \quad \langle 1\,0\,0\rangle$$

The theoretical torsional stiffness, defined as $k_t \equiv \partial\tau/\partial\beta$, is compared against simulation data in Tables 1–3. The agreement for aluminum is generally good for all three directions, with an error around 10%. The agreement between theory and simulation is not that good for gold, with errors around 30%. This disagreement persists at 0 K, but disappears if the torsional stiffness is calculated without letting the atoms relax between subsequent twists. These expressions are derived assuming that the cross-sections remain planar and circular. However, the shear modulus varies throughout the cross-section due to elastic anisotropy. Hence, cross-sections may become non-planar or non-circular, leading to discrepancies. This hypothesis is supported by agreement achieved when the wire is not allowed to relax which forces the cross-sections to remain planar and circular. Another source of error is the uncertainty in the calculation of the radius. However, we note that the effective stress strain curves shown in Figs. 2, 7, and 10(c), (d) collapse on one another in the linear range suggesting a lack of radius dependence.

3.1. $\langle 1\,1\,0\rangle$ Orientation

If we define a yield strain $\gamma_Y = \beta_Y R$ at which the curve first unloads, then the yield strain appears size independent for wires oriented along $\langle 1\,1\,0\rangle$, as shown in Table 1. The average and standard deviation of the yield strain are taken from eight different runs for each case reported. Fig. 2(a) and (b) shows three sample twisting and untwisting curves for both metals at a diameter of 5 nm. Fig. 2(c) and (d) show an effective shear stress–strain response of the material for the three different diameters. The strain is the engineering surface shear strain and the effective stress is the torque divided by the radius cubed, which removes and dependence on the radius of the wire.

The strength of the materials is not the only aspect of the deformation that depends on the wire material. Figs. 3 and 4 show the evolution of plastic deformation in $\langle 1\,1\,0\rangle$ oriented nanowires. As discussed previously by the authors

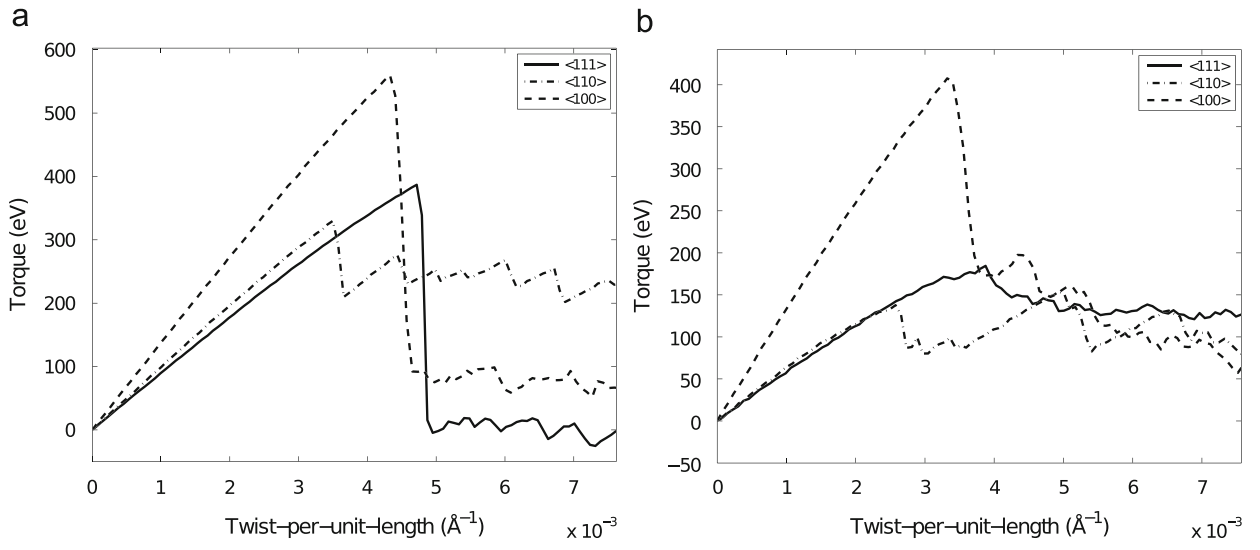

Fig. 1. Torque–twist per unit length curves for three different orientation 5 nm diameter (a) aluminum and (b) gold nanowires.

Table 1
Yield strains and torsional stiffnesses for ⟨1 1 0⟩ oriented metallic nanowires.

Material	Diameter (nm)	γ_Y	k_t (eV Å)	k_t (theory)
Gold	5	0.061 ± 0.002	$(6.75 \pm 0.25) \times 10^4$	1.02×10^5
Gold	7.5	0.056 ± 0.001	$(3.41 \pm 0.04) \times 10^5$	5.19×10^5
Gold	10	0.057 ± 0.002	$(1.08 \pm 0.004) \times 10^6$	1.64×10^6
Aluminum	5	0.085 ± 0.002	$(1.02 \pm 0.004) \times 10^5$	1.10×10^5
Aluminum	7.5	0.078 ± 0.002	$(5.24 \pm 0.02) \times 10^5$	5.56×10^5
Aluminum	10	0.078 ± 0.001	$(1.65 \pm 0.003) \times 10^6$	1.77×10^6

The yield strain $\gamma_Y = \beta_Y R$ is calculated when the torque initially begins to unload. The torsional stiffness is $k_t = \frac{\partial \tau}{\partial \beta}$ and the averages and standard deviations are reported for 8 different runs.

Table 2
Yield strains and torsional stiffnesses for ⟨1 1 1⟩ oriented metallic nanowires.

Material	Diameter (nm)	γ_Y	k_t (eV Å)	k_t (theory)
Gold	5	0.093 ± 0.003	$(6.19 \pm 0.05) \times 10^4$	8.68×10^4
Gold	7.5	0.085 ± 0.001	$(2.95 \pm 0.03) \times 10^5$	4.40×10^5
Gold	10	0.082 ± 0.002	$(9.79 \pm 0.09) \times 10^5$	1.39×10^6
Aluminum	5	0.119 ± 0.003	$(9.06 \pm 0.05) \times 10^4$	1.07×10^5
Aluminum	7.5	0.105 ± 0.002	$(4.83 \pm 0.01) \times 10^5$	5.41×10^5
Aluminum	10	0.097 ± 0.003	$(1.53 \pm 0.003) \times 10^6$	1.71×10^6

Table 3
Yield strains and torsional stiffnesses for ⟨1 0 0⟩ oriented metallic nanowires.

Material	Diameter (nm)	γ_Y	k_t (eV Å)	k_t (theory)
Gold	5	0.082 ± 0.005	$(1.38 \pm 0.004) \times 10^5$	1.49×10^5
Gold	7.5	0.080 ± 0.002	$(6.62 \pm 0.02) \times 10^5$	7.56×10^5
Gold	10	0.074 ± 0.002	$(2.11 \pm 0.004) \times 10^6$	2.39×10^6
Aluminum	5	0.113 ± 0.003	$(1.39 \pm 0.003) \times 10^5$	1.21×10^5
Aluminum	7.5	0.112 ± 0.003	$(7.02 \pm 0.02) \times 10^5$	6.13×10^5
Aluminum	10	0.112 ± 0.006	$(2.14 \pm 0.002) \times 10^6$	1.94×10^6

(Weinberger and Cai, 2010), the gold nanowires deform mainly by nucleation of partial dislocations with the stacking faults terminating at the wire surface. In contrast, the aluminum wires start by nucleating partial dislocations, but the trailing partials follow creating perfect screw dislocations in the wire. For 5 nm diameter aluminum wires and 20 nm diameter gold nanowires, we see a mixture of both partial and perfect dislocations. The difference in nucleating perfect and partial dislocations is related to the material's stacking fault energy and the radius of the nanowire. The stacking fault energy of the gold potential is 31 and 146 mJ/m^2 for the aluminum potential. This results in a equilibrium partial dislocation separation of approximately 1.5 and 0.3 nm in bulk gold and aluminum, respectively.

The nucleation of dislocations generally occur, in these simulations, on planes of maximum shear stress. A simple consideration of the torsion of a circular cross-section shows that two types of planes contain the maximum shear stress. Planes perpendicular to the wire axis are planes of maximum stress as well as all planes that contain the wire axis. In the case of a ⟨1 1 0⟩ oriented nanowire, two {1 1 1} type planes contain the specific ⟨1 1 0⟩ direction, separated by 71°, and are likely planes for dislocation activity. This is confirmed by examination of the planes of slip in Fig. 3.

The twisting and untwisting curves for gold in Fig. 2(b) show a large amount of, and often complete, reversibility during untwisting. Since the torque in the untwisting curves of gold generally do not drop below zero, this means that the dislocations all leave prior to unloading. The torque, in a few cases, does drop below zero, but it is difficult to determine if this is caused simply by fluctuations in the torque calculation, or a real unloading. Regardless, in every case the gold wires are always able to recover a significant amount of the deformation. For the case of aluminum, Fig. 2(a), we can see that the deformation is always irreversible. If one wishes to remove all the dislocations from the wire, a negative torque must be applied to the wire in order to accomplish this. The reversibility of the gold nanowires should be size dependent, though. As we will see later, perfect dislocations are generally stable inside a wire, making the deformation generally irreversible. As the wire diameter increases the amount of perfect dislocations that nucleate will increase, transitioning from reversible to irreversible deformation.

3.1.1. Stability analysis

The difference between perfect and partial dislocations in gold and aluminum illustrates that nucleation should depend on the stacking fault energy of the material and the diameter of the nanowire. This suggests that the difference in

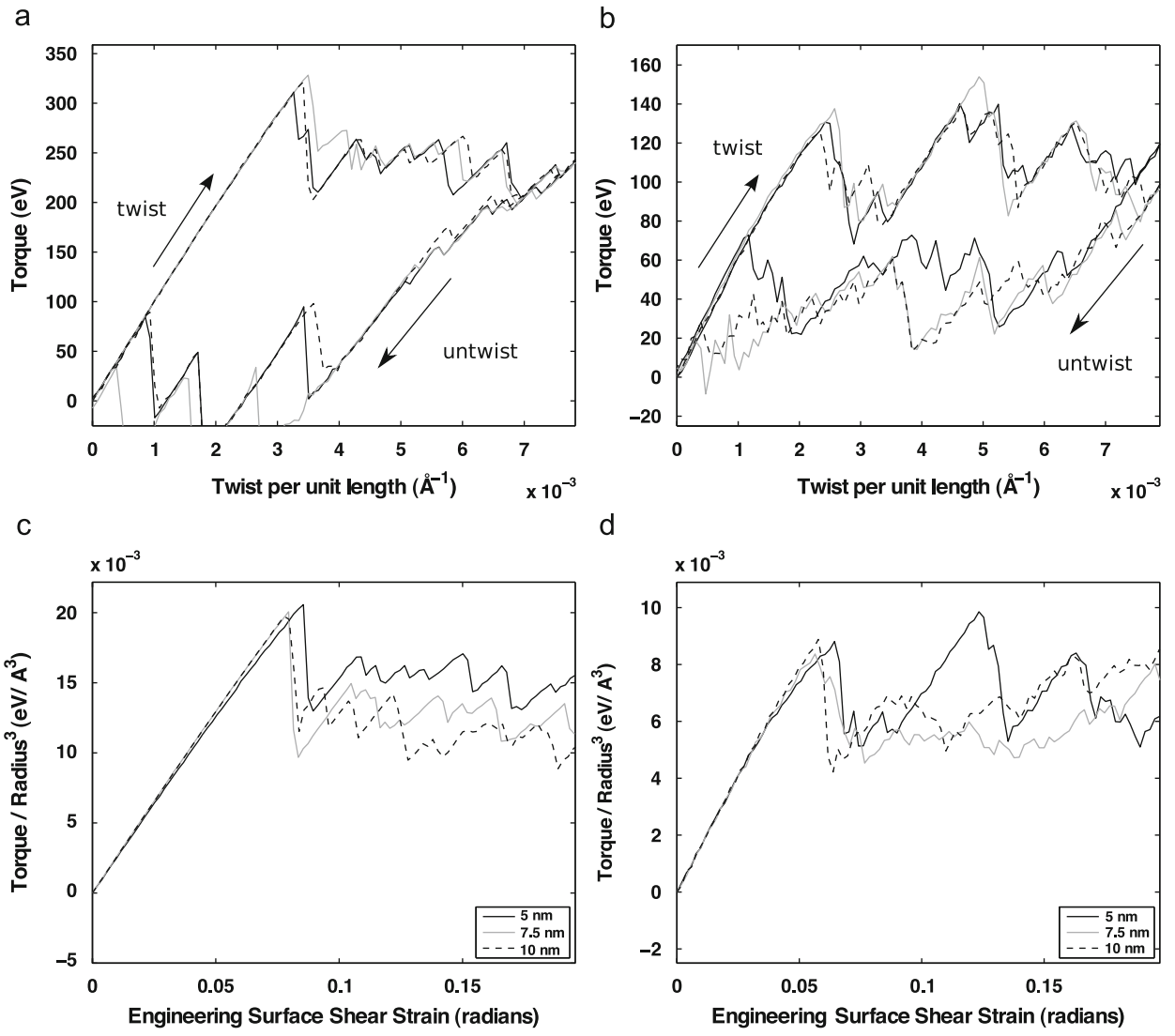

Fig. 2. Three representative torque twist curves showing both loading and unloading, (a) aluminum and (b) gold nanowires with 5 nm diameters. Torsional stress–strain curves (c) for aluminum and (d) for gold, which illustrate the effect of diameter on mechanical properties.

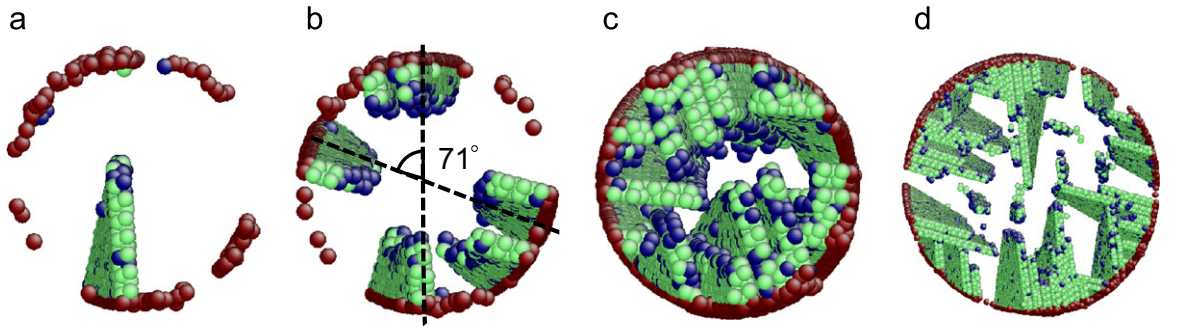

Fig. 3. The evolution of dislocation networks in ⟨1 1 0⟩ gold nanowires. (a) The initial plastic event, (b) more partial dislocations nucleate and (c) significant dislocation structure once loading is complete for a 7.5 nm diameter wire. (d) A similar network in a 20 nm diameter wire showing mostly partial dislocations with a few perfect dislocations. The engineering surface shear strains for the configurations are: (a) 0.062, (b) 0.084, (c) 0.200, and (d) 0.192.

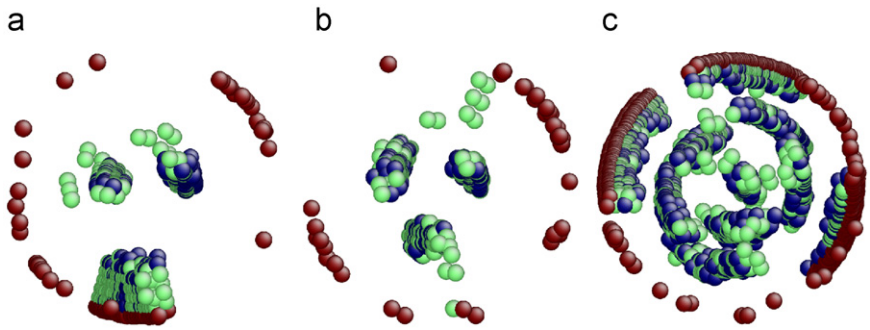

Fig. 4. The evolution of a dislocation network in a ⟨1 1 0⟩ aluminum nanowire. (a) Perfect and partial dislocations, (b) nucleated perfect dislocations and (c) the final configuration. The engineering surface shear strains for the configurations are: (a) 0.108 (b) 0.118, and (c) 0.200.

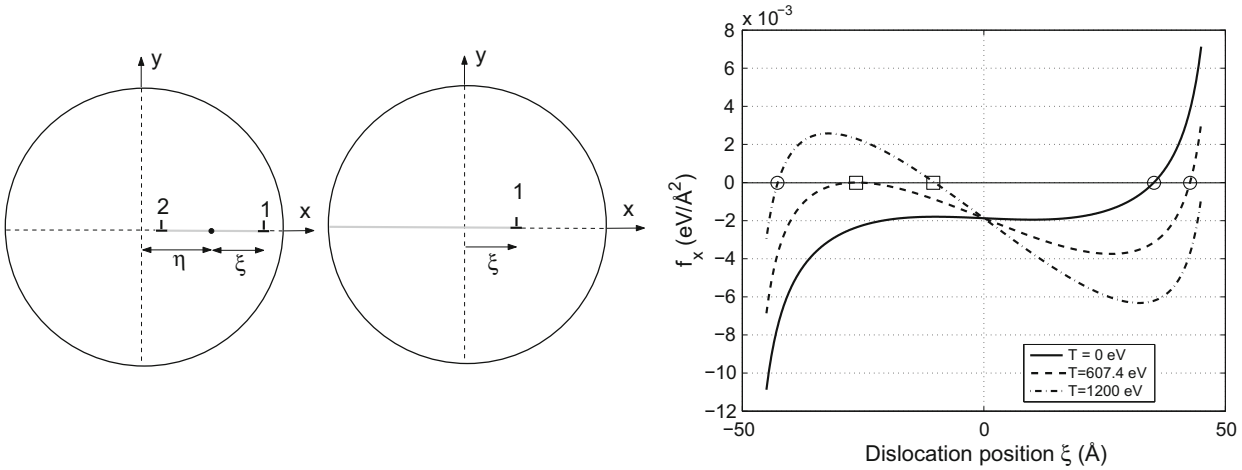

Fig. 5. The configuration for (a) two partial dislocations and (b) one partial dislocation in a cylinder and (c) the forces on one dislocation in a cylinder. Unstable equilibrium points are marked with a circle and stable equilibrium points are marked with a square.

nucleation may be explained purely through elastic effects and, that at some critical diameter, the dislocations are no longer stable in the nanowire. A simple analytical model can be constructed involving two partial dislocations in a cylinder separated by a stacking fault, as shown in Fig. 5(a). The forces on the dislocations and their stability can be written using the expressions developed by Eshelby (1979) as discussed in Appendix A. From this analysis we find that the partial pair is only stable when their center of mass is at the center of the nanowire. A positive applied torque simply pushes the partials closer together and enhances the stability of the configuration. Two negative critical torques can be established. One pulls the partials out leaving a stacking fault. The other makes the configuration unstable with respect to perturbations of the center of mass, resulting in the partial pair leaving together. The lower critical torque, from numerical investigations, appears to always be the center of mass instability. This makes sense since the wire containing a stacking fault will have a higher energy than the defect free wire.

This problem is very similar to the problem Eshelby (1953) solved which showed that perfect screw dislocations are stable inside whiskers. However, we now have two partial dislocations bounded by a stacking fault inside a cylinder. For the perfect screw dislocation problem, Eshelby was able to show that an applied torque drives the screw dislocation out when it reaches a critical value of $\tau = -\frac{1}{4}\mu b R^2$. We can compare this to our solution for a screw dislocation dipole in gold with $\mu = 31$ GPa, $\nu = 0.4$, $b = 2.88$ Å, $b_e = 0.83$ Å, $b_s = 1.44$ Å, $\gamma = 30\,\mathrm{mJ/m^2}$ and the radius is taken to be R=25 Å. The critical torque predicted by our analysis is $\tau^{\mathrm{crit}} = -53.6$ eV while Eshelby's result gives $\tau^{\mathrm{crit}} = -87.2$ eV. This shows that the dissociated dislocation is less stable than a non-dissociated perfect dislocation. This can be compared with the critical torque to pull two partial dislocations out of the wire in opposite directions, −169 eV, whose magnitude is much higher. As the diameter of the wire increases, the critical torque approaches that predicted by Eshelby; at a radius of 50 Å we find the critical torques are −306 eV and −349 eV for this analysis and Eshelby's, respectively. This shows that the partial dislocation pairs behave as perfect dislocations for all but the smallest nanowires.

The above model is unable to explain why at smaller diameters only partial dislocations nucleate because it predicts that a partial dislocation pair is also (meta-)stable in torque free nanowires. However, elasticity models can help explain why the deformation in gold nanowires is reversible but not is in aluminum. This is because a pair of partial dislocations

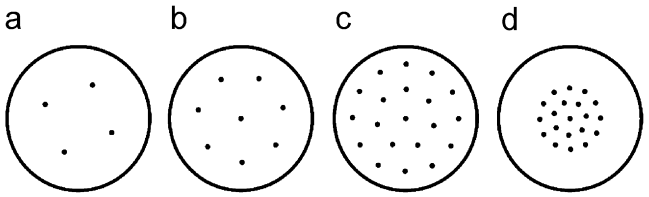

Fig. 6. The equilibrium structure of (a) 4, (b) 8, and (c) 20 dislocations in a torque free cylinder and (d) 20 dislocations under an applied torque. The patterning of these dislocations illustrates the homogeneity of the deformation.

(connected by a stacking fault) is meta-stable in the torque-free wire while a single partial dislocation is not. The force on a single partial dislocation shown in Fig. 5(b) is

$$f_x^1 = \frac{\mu b_e^2}{2\pi(1-\nu)}\frac{\xi}{R^2-\xi^2} + \frac{\mu b_s^2}{2\pi}\left[\frac{\xi}{(R^2-\xi^2)} - \frac{2\xi(R^2-\xi^2)}{R^4}\right] - \gamma - \frac{2}{\pi}\frac{\xi}{R^4}b_s\tau \tag{1}$$

and is plotted in Fig. 5(c). For zero torque, the partial dislocation has one equilibrium position for which $\xi > 0$. This position is an unstable equilibrium since the slope at the point is positive, which results in a negative second derivative of the energy. It is possible, just as it was for the pair of partials, to determine the torque required to make the dislocation stable using similar criterion. The dislocation is stable when $f_x^1 = 0$ and $\partial f_x^1/\partial\xi < 0$. The critical torque can be found by requiring $f_x^1 = 0$ and $\partial f_x^1/\partial\xi = 0$. The critical torque to stabilize the partial dislocation is now positive and has a value of 607 eV. This shows that a single partial dislocation is unstable in a torque free wire. Therefore, when the wire is unloaded in our MD simulations, perfect dislocations already in the wire remain and provide a plastic twist. However, if only the leading partial dislocations nucleate, they are unstable and will leave during the unloading process, creating a reversible torque twist curve.

3.1.2. *Dislocation patterning*

The deformation shown in Fig. 4 and discussed previously shows striking homogeneity. This has important implications for plastic metal forming at the micro and nanoscales. To better understand this process, we need to predict how more dislocations will distribute in the wire during deformation. This can be done using a two dimensional dislocation dynamics code as described previously. In this model, every dislocation will be modeled as a like signed perfect screw dislocation and will be initially placed in the cylinder at a random location within 0.5 of the radius (so that they do not escape). The resulting equilibrium configurations are shown in Fig. 6. A simple ring structure appears stable when the number of dislocations is about 6 or less. When there are 6 or more dislocations, one dislocation will occupy the center position. A large number of dislocations shows more complicated ring structures, as in Fig. 6(c). Barnett and Nix (Private communication) have shown that a ring of N dislocations is always in equilibrium in a torque-free cylinder. When our DD simulations are carried out, the ring structure appears to be an unstable equilibrium for N greater than 6 and numerical noise changes the structure to one or more dislocations inside the outer ring. This patterning shows that as more dislocations are nucleated, they spread out ensuring the deformation continues in a homogeneous fashion.

The patterning shown in Fig. 6 results from allowing the dislocations to move along the direction of the Peach–Koehler force. As shown in our MD simulations, the dislocations appear confined to slip planes and may not be able to reach these equilibrium positions. That may influence the resulting patterning seen in MD simulations and what would be observed in experiments. Furthermore, the application of torque tends to drive the dislocations into the interior of the wire, as shown in Fig. 6(d). Therefore, the completely disperse configuration shown in Fig. 6(c) should not always be expected. Finally, these simulations show that an arbitrarily large number of screw dislocations can be in equilibrium in a torque free wire.

3.2. ⟨1 1 1⟩ *Orientation*

For a ⟨1 1 1⟩- oriented wire a {1 1 1} type plane is oriented perpendicular to the wire axis, which as discussed before, is a plane of maximum stress. This suggests that this plane will be the most active slip plane during plastic deformation. For these nanowires, the trend shown in Table 2 is that smaller is stronger. The stress required for nucleation decreases as a function of the wire diameter. We also see that aluminum is again stronger than gold in this orientation.

Fig. 7 shows the twisting and un-twisting curves for the ⟨1 1 1⟩ oriented nanowires in addition to the normalized stress–strain curves. The un-twisting part of the curves show that the deformation is essentially irreversible. These figures also illustrate an important difference between the gold and aluminum torque twist curves. When the aluminum wires yield, the torque relaxes to nearly zero almost instantaneously. Gold, however, unloads more slowly reaching a near zero torque condition close to the end of the simulations. This behavior correlates well with the dislocation network formation. When aluminum wires yield, the dislocations nucleate and organize into structures while the torque drops. By the time the torque is completely relaxed, a high angle twist boundary has already formed. However, in gold, the dislocation structures

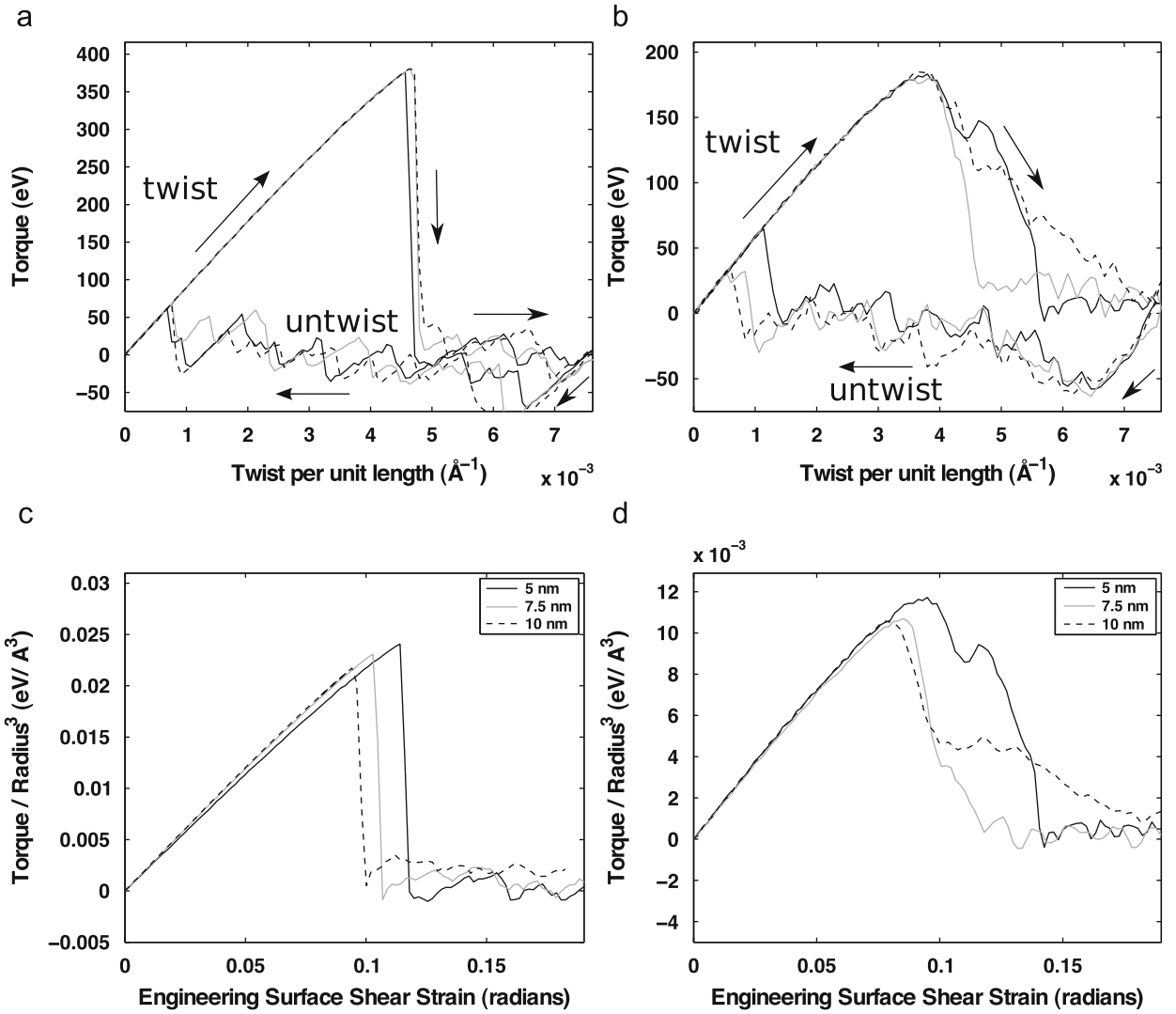

Fig. 7. Three representative torque twist curves showing both loading and unloading for ⟨1 1 1⟩ oriented (a) aluminum and (b) gold nanowires. Torsional stress–strain curves (c) for aluminum and (d) for gold, which illustrate the effect of diameter on mechanical properties.

take longer to nucleate and organize, so the torque stays higher for much longer. This can be attributed to the higher torque when dislocations first nucleate in aluminum compared to gold.

3.2.1. Dislocation patterning

The strength of the wires may depend weakly on the diameter, however we do not see a great difference in the behavior of the dislocations that emerge from the deformation. The deformation is limited to one or just a few planes, localizing the deformation. The dislocation structure that evolves initially starts by the creation of a Y junction shown in Fig. 8(a) and (b). The junction starts from the nucleation of a single partial dislocation. As the partial dislocation expands, it eventually nucleates two trailing partial dislocations, which covers all three possible partial dislocations on that glide plane. This structure, as seen in Fig. 8(b), is all that is needed to evolve into a extended Y junction. Fig. 8(b) and (c) also shows that constricted Y junctions can form from the interaction of two dislocations. Our simulations show that both constricted and extended nodes can form as the initial embryo of the twist boundary. However, a Y junction of screw dislocations is the first step in the twist boundary formation.

As the dislocation structure evolves, it develops into a {1 1 1} twist boundary shown in Fig. 8(d). The clarity of this figure is unique since in most our simulations partial dislocations nucleated on parallel planes close to the twist boundary restrict visualization. The larger diameter wires, such as the 17.5 nm in diameter shown, illustrate the difference between constricted and extended nodes better. But, this also makes visualization of the hexagonal structure more difficult. Fig. 8(d) shows a hexagonal structure during untwisting in a 5 nm diameter aluminum wire. Careful examination of this network

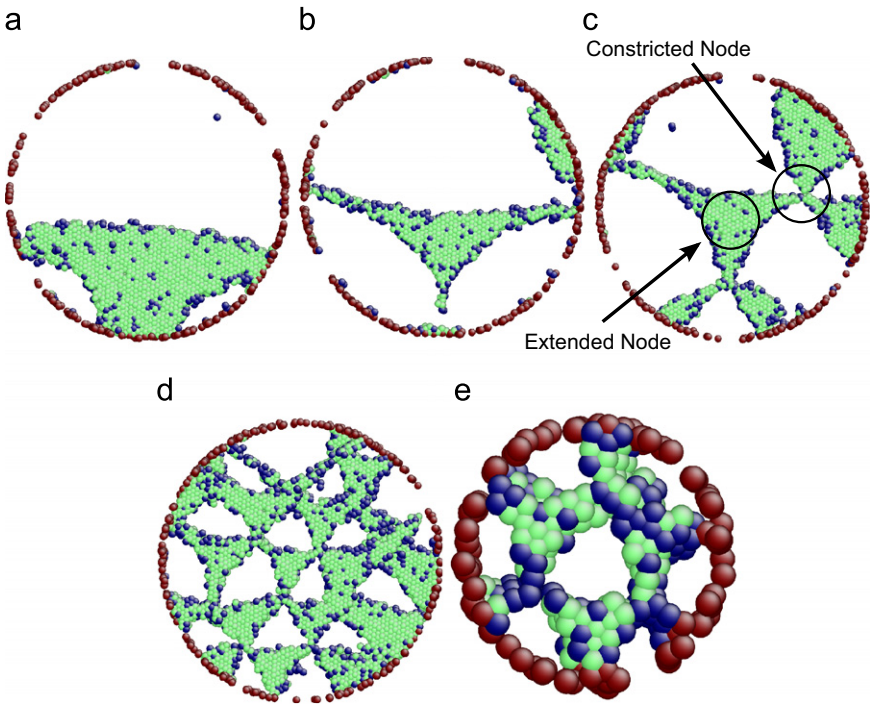

Fig. 8. The evolution of dislocation networks in ⟨1 1 1⟩ gold nanowires. (a) Initial nucleation of three partial dislocations in a 17.5 nm diameter gold wire, (b) The initial formation of an extended Y junction, (c) the formation of a constricted node, (d) evolution to a hexagonal dislocation array of alternating constricted and extended junctions, (e) a hexagonal network in a 5 nm aluminum nanowire viewed during untwist. The engineering surface shear strains for the configurations are: (a) 0.072, (b) 0.074, (c) 0.076, (d) 0.098, and (e) 0.038.

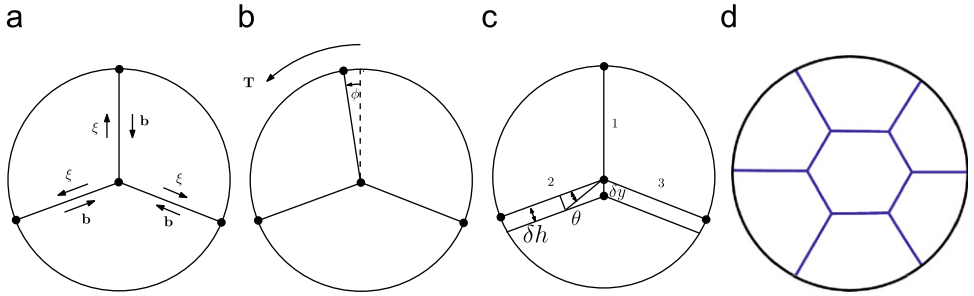

Fig. 9. (a) Symmetric screw dislocation junction and (b) the perturbed configuration of one arm by an angle ϕ, (c) the perturbed configuration of the center node by δy, (d) a stable hexagonal array from DD simulations.

also shows the same nodal configuration, however it is more visible due to a combination of a smaller density network and the constriction of the partials caused by the torque.

For single crystal wires in torsion, McClintock and Prinz (1983) proposed a mechanism by which such a network would evolve. The first junction in our simulations, the Y junction, forms by the reaction they postulate in their paper. But, the evolution of further dislocation structures occurs differently. They hypothesize that network formation requires a number of sources set in the right places to form the hexagonal dislocation network including some sources on the interior of the wire. In our MD simulations, the sources of the dislocation are always on the surface. There are no pile ups as suggested by McClintock and Prinz (1983) since all the dislocations needed for the structure naturally nucleate off the surface.

3.2.2. *Stability analysis*

The screw dislocation Y junction obtained in this configuration should be stable under an applied torque as an array of like signed screw dislocations. This idea can be confirmed by doing a simple stability analysis of the structure. Consider a symmetric array of three left handed screw dislocations as shown in Fig. 9(a). The array is unstable when there is no applied torque since any perturbation of the center node will cause a junction to zip, leaving one screw dislocation in the cylinder. However, if a torque is applied to the cylinder as shown in Fig. 9(b), the Y junction is stabilized.

In order to understand how the dislocation structure is stabilized we analyze a perturbed state shown in Fig. 9(b). The Peach–Koehler force exerted on the vertical segment as it is displaced from the screw orientation by an angle ϕ is

$$\mathbf{f} = -\frac{\tau br}{J}(\sin\phi\cos\phi\hat{\mathbf{x}} + \sin^2\phi\hat{\mathbf{y}}) \tag{2}$$

where b is the magnitude of the Burgers vector, τ is the applied torque, J is the polar moment of inertia and r is the radial distance. For $\phi \ll 1$, this reduces to

$$\mathbf{f} = -\frac{\tau br}{J}\phi\hat{\mathbf{x}} \tag{3}$$

which is a restoring force opposite to the direction of ϕ. Of course, if the array were composed of right handed screw dislocations instead, then $b<0$ and the force is destabilizing. The force would also be destabilizing for a left handed screw array with a negative applied torque.

The perturbation of one of the arms by an angle ϕ illustrates the stabilizing nature of the applied torque. However, the dislocation arm would also tend to rotate back by a line tension argument. This is because the rotated arm has a higher energy since it has an edge component. In addition, the previous analysis does not predict a critical torque to stabilize the junction. This can be done by considering another perturbed configuration shown in Fig. 9(c) where the center node is moved by a distance δy without changing the arm angles. To first order in δy, the line length of the junction does not change. The work done by the applied torque is zero to first order, which is the Peach–Koehler force on the unperturbed configuration. Therefore, to investigate the critical torque, the configuration must be analyzed to second order in δy, which is done in detail in Appendix B. The critical torque is

$$\tau_c = \frac{R^2\mu b}{8}\log\left(\frac{R}{b}\right) \tag{4}$$

A hexagonal network, like the one shown in Fig. 9(d), will have a critical torque as well. This is the torque required to keep the hexagonal structure inside the wire diameter. Lowering the torque would allow the structure to dissolve, while increasing it will simply create a more compact hexagon. If we approach the problem using line tension arguments as above, we find that the change in energy is zero. This is because as the hexagon enlarges, the change in perimeter always exactly matches the loss of length in the spokes. However, if we account for the elastic interactions, the structure would be unstable at zero torque due to the repulsion of the like-signed screw dislocations. The repulsive Peach–Koehler force can be approximated by assuming the screw segments in the hexagon interact as straight infinite segments with a force $f = \mu b^2/4\pi r$ where r is half the distance between them. The applied torque provides a stabilizing force of $f = -\tau rb/J$. Equating forces and solving for the torque gives $\tau = \mu Jb/4\pi r^2$. From this simple model we estimate the critical torque in terms of R by setting $r=R$ and assuming a simple constant of proportionality

$$\tau_c = \alpha\frac{\mu Jb}{4\pi R^2} = \alpha\frac{\mu bR^2}{8}$$

The critical torque for the hexagonal loop is very similar in form to that of the Y junction. One could also propose such a form based on dimensional analysis since the torque must be proportional to the shear modulus times the Burgers vector and the R^2 term comes from the only available length scale parameter in the problem.

The stability of these structures is further confirmed using dislocation dynamics. The screw dislocation array shown in Fig. 9(a) is a stable equilibrium structure in DD under an appropriate applied torque. A Y junction is created and the center node is moved down as part of the initial structure. Reversing the direction of the torque causes the structure to dissolve, in agreement with the above calculations. Fig. 9(d) shows a hexagonal structure in dislocation dynamics, which is also stabilized by an applied torque. In our dislocation dynamics simulations, the hexagonal array dissolves when the applied torque is removed. We note that in a real crystal, the twist boundary may be stabilized (even at zero applied torque) by impurities or other defects.

3.3. ⟨100⟩ Orientation

The ⟨100⟩ is a high symmetry direction and has been the subject of intensive investigations of size effects in micropillars. The orientation is the highest symmetry direction in uniaxial loading involving the most possible slip systems. However, we note that based on a qualitative look at the associated stress strain curves, it appears similar to the ⟨111⟩ direction. Fig. 10(a) and (b) shows the torque twist curves for both aluminum and gold for 5 nm diameter wires and we note a similar significant drop in the torque upon dislocation nucleation. However, it is not clear if there is a trend to the strength of the nanowires as a function of diameter, as illustrated in Fig. 10(c) and (d). The yield strain of the wires from Table 3 shows a slight decrease in strength for gold, but not as strong or obvious as the ⟨111⟩ direction. The strength of the wires for aluminum remains constant, independent of diameter.

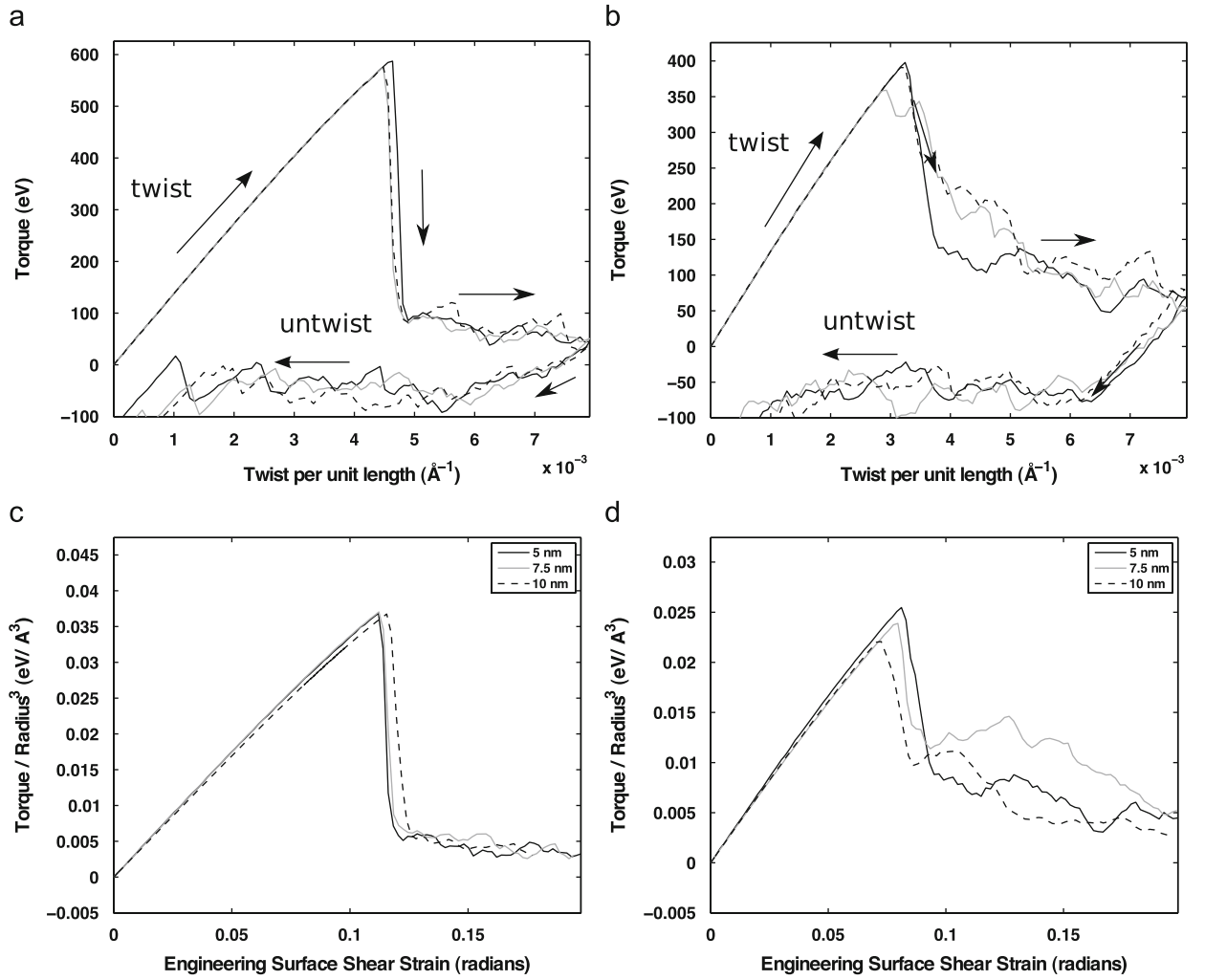

Fig. 10. Representative twisting and un-twisting curves for 5 nm diameter (a) aluminum and (b) gold nanowires. Torsional stress–strain curves (c) for aluminum and (d) for gold, which illustrate the effect of diameter on mechanical properties.

3.3.1. *Dislocation patterning*

The deformation of the wire after initial failure shows the formation of a twist boundary, similar in some respects to the $\langle 1\,1\,1 \rangle$ direction. Fig. 11 shows the nucleation of dislocations and their evolution into a twist boundary. The dislocations behave effectively the same in both aluminum and gold. In larger diameters, the initial dislocations that are originally nucleated show splitting of the dislocations into partials, but eventually the dislocations organize into planar structures with constricted perfect dislocations. This is interesting, especially in the case of gold, because the partial separation in the bulk should be around 1.5 nm, which is on the same order of the diameters of the wires. However, the applied torque both constricts the partials and drives them to organize onto planes of maximum stress. Furthermore, the dislocations organize themselves into perfectly straight rectangular arrays, which is classical model of a low angle twist boundary (Hirth and Lothe, 1982).

The twist boundary that forms should be a rectangular array of screw dislocations. For a wire oriented along the [0 0 1] direction, the screw dislocations that can form such a boundary are $a/2[1\,1\,0]$ and $a/2[1\,\bar{1}\,0]$, each of which can exist on two slip planes. These slip planes are the $(1\,\bar{1}\,1)$ and $(1\,\bar{1}\,\bar{1})$ for the $a/2[1\,1\,0]$ and the $(1\,1\,1)$ and $(1\,1\,\bar{1})$ for the $a/2[1\,\bar{1}\,0]$ respectively. All of these slip systems can be active, but a regular rectangular array is needed to form a pure twist boundary.

The slip geometry also implies that it is possible to form many twist boundaries from the nucleation of dislocations at various locations along the wire diameter. If dislocations nucleate far enough from the twist boundary, they would either form a new twist boundary or have to cross-slip to reach a currently forming boundary. Fig. 11(d) shows a perspective view of the plasticity along a 10 nm diameter gold nanowire. In this case, dislocations initially nucleate and form multiple twist boundaries, as expected. Secondary twist boundaries are often observed, but usually are made of only two or three dislocations. Further plastic deformation is limited to the primary twist boundary which eventually evolves into a high angle twist boundary.

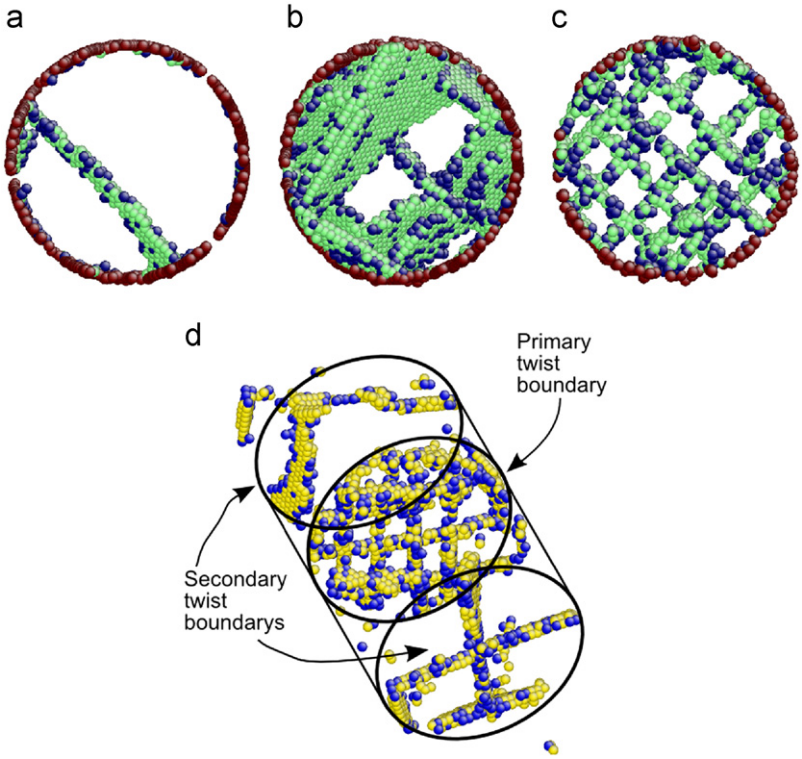

Fig. 11. The evolution of a dislocation network in a ⟨100⟩ 10 nm gold nanowire. (a) Initial dislocations nucleated in the wire, (b) the dislocations organize onto planes, (c) and form a single rectangular array. (d) Primary and secondary twist boundaries that form along the wire. The primary boundary is the same boundary as that shown in (c). The engineering surface shear strains for the configurations are: (a) 0.076, (b) 0.082, and (c) 0.096.

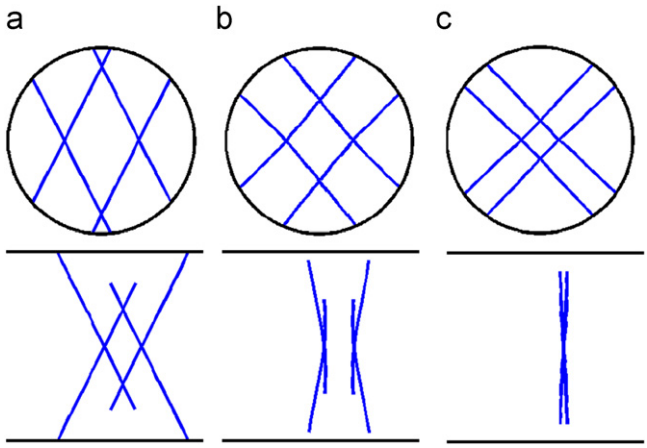

Fig. 12. The evolution of a (100) twist boundary from a random arrangement of dislocations. (a) The initial arrangement of dislocations. (b) An intermediate configuration where they are in a nearly square configuration but not on the same plane. (c) The final configuration showing a planar rectangular array of screw dislocations.

It is generally believed that the low angle twist boundary will form from dislocation motion under the applied torque. This suggests that the organization of the dislocations is largely based on elasticity. To test this theory, dislocation dynamics is used to simulate a wire under torsion. However, since dislocation dynamics cannot model nucleation, we start with an initial dislocation array. We choose to model four dislocations, two with each Burgers vector described above and on each of the individual slip planes. The dislocations are then allowed to move on their glide planes until equilibrium is reached. The evolution of the

dislocation structure is shown in Fig. 12. The simulations shows that under an applied torque, the dislocations rotate to screw orientation, form a grid, and eventually move onto the same plane, perpendicular to the wire axis.

4. Discussion

The issue of strain rate is always important in MD simulations since high strain rates ($\sim 10^8\,s^{-1}$) cannot be avoided. Certainly the strain rate will affect the strain at which the dislocation nucleate (Zhu et al., 2008). However, the more important question is whether the high strain rate changes the deformation mechanism. To address this question, we have first carried out simulations with the number of time steps increased from 5000 to 25 000 for 5 nm diameter gold nanowires. This drops the strain rate from nominally 4×10^8 to 8×10^7 and there are no changes in deformation mechanisms. Of course, a brute force approach is limited by computer resources. That is why it is important to note that the mechanisms by which the structures dissolve are the same when they form. During the dissolution, the applied torque is usually much lower than when the dislocations originally nucleate, showing that their occurrence is not due to the high stresses. Furthermore, dislocation dynamics simulations also support the structures that form and are in agreement with classical models. This suggests that our results are not strongly dependent on the applied strain rate.

The results presented here are for pristine wires without surface or other defects. A question that arises is how surface defects affect the homogeneity of the deformation. We expect that defects will cause the deformation to be come more heterogeneous, localized around the defect. To address this we have also carried out simulations of 5 nm diameter gold nanowires with surface vacancies where 6 atom clusters were removed on the wire surface. The results show that the vacancy clusters are where dislocations originally nucleate, as commonly expected. However, since the $\langle 1\,1\,1\rangle$ and $\langle 1\,0\,0\rangle$ oriented nanowires already show heterogeneous deformation, it does not change the deformation mechanisms. For the $\langle 1\,1\,0\rangle$ orientations, the dislocations start to nucleate at the vacancies, but also nucleate at other sites later in the deformation. Even if a vacancy was a continued site for nucleation for perfect dislocations, it would still likely result in homogeneous deformation since the nucleated dislocations would spread out in the interior, as illustrated in our DD simulations. Thus, while surface defects can act as preferential sites for nucleation, they do not tend to alter the plastic deformation that occurs.

Even though the wires are under (torsional) periodic boundary conditions along their length, the question of length does arise. In our simulations the length of the wire was twice the diameter, or an aspect ratio of two. Simulations were also carried out for wires that are twice as long, for aspect ratios of 4. These simulations also show no change in the mechanisms of plastic deformation. The deformation for the $\langle 1\,1\,0\rangle$ and $\langle 1\,1\,1\rangle$ are essentially limited to a plane, so the length would appear to have little effect. For the $\langle 1\,0\,0\rangle$, we may expect to see a few more dislocations along its length if initial nucleation does not occur near a single boundary. However, after a boundary forms, further deformation occurs only on this boundary regardless of length.

These simulations show that wires under torsion can deform either through the formation of twist boundaries, as expected, or through coaxial or Eshelby dislocations. When the deformation is through coaxial dislocations, the deformation is homogeneous and potentially reversible if the wires are small enough to nucleate only partial dislocations. Furthermore, $\langle 1\,1\,0\rangle$ wires deform in such a way that they maintain a significant fraction of their strength while in other directions there is a significant strength loss.

This orientation dependent plasticity under strain gradients has important implications for strain gradient theories. This work suggests that different dislocation networks can form, with different densities, that all accomodate the plastic twist but depend only on wire orientation. Orientation dependent strain gradient plasticity models, as suggested by these results, may overcome some of the limitations of existing theories (Kubin, 2003).

There is no reason to expect that these results, except for reversibility, should be limited to nanowires. Since the mechanisms do not appear to be size dependent, we expect the results to be applicable to single crystal microwires as well, as long as the wires are initially dislocation free. The existence of initial dislocation networks may alter how the wires deform, since networks will likely evolve out of the multiplication of the statistically stored dislocations inside the wires. Dislocation dynamics simulations can help answer these questions in the future.

5. Conclusion

We have shown that the plasticity of pristine single crystal FCC metallic wires in torsion is orientation dependent. For wires oriented along the $\langle 1\,1\,0\rangle$, coaxial dislocation nucleate causing the plasticity to be homogeneous. For the $\langle 1\,1\,1\rangle$ and $\langle 1\,0\,0\rangle$ orientations, twist boundaries form which localizes the deformation. The $\langle 1\,1\,0\rangle$ wires also maintain a significant fraction of their strength after yield, while the other directions lose most of their strength.

When $\langle 1\,1\,0\rangle$ wires are small enough, only partial dislocations nucleate and the deformation becomes reversible since partial dislocations are unstable in torque free wires. For thick $\langle 1\,1\,0\rangle$ wires, perfect dislocations nucleate and our DD simulations show that many screw dislocations can co-exist in the wire even in a torque-free state. For $\langle 1\,1\,1\rangle$ wires, the hexagonal dislocation network that forms the twist boundary is stable in the wire only when the applied torque exceeds a critical value. Finally, DD simulations show that rectangular dislocation networks in $\langle 1\,0\,0\rangle$ wires can be formed by rotation of existing dislocations under the inhomogeneous stress field from the applied torque.

Acknowledgments

The work is supported by National Science Foundation Career Grant CMS-0547681, and Air Force office of Scientific Research/Young Investigator Program grant, the Army High Performance Computing Research Center at Stanford, and a Benchmark Stanford Graduate Fellowship (to C.R.W.).

Appendix A. The stability of a partial dislocation pair

This appendix addresses the stability of a partial dislocation pair in a wire. The wire lies along a $\langle 1\,1\,0\rangle$ direction and the two partial dislocations will have equal and opposite edge components, b_e and equal screw components, b_s. The force on the two dislocations can be written in terms of their center of mass and separation distances as shown in Fig. 5(a). The edge components of dislocations 1 and 2 are b_e and $-b_e$, respectively. The force on dislocation 1 is

$$f_x^1 = \frac{\mu b_e^2}{2\pi(1-\nu)}\left[\frac{\eta+\xi}{R^2-(\eta+\xi)^2} + \frac{(\eta-\xi)((\eta-\xi)(\eta+\xi)-R^2)^2 - 2R^2\xi((\eta-\xi)(\eta+\xi)-R^2) - 4(\eta-\xi)R^2}{(R^2-(\eta+\xi)^2)^3} - \frac{1}{2\xi}\right] + \frac{\mu b_s^2}{2\pi}\left[\frac{\eta+\xi}{R^2-(\eta+\xi)^2} + \frac{\eta-\xi}{R^2+(\eta+\xi)(\eta-\xi)} + \frac{1}{2\xi} - \frac{2(\eta+\xi)(R^2-(\eta+\xi)^2)}{R^4} - \frac{2(\eta+\xi)(R^2-(\eta-\xi)^2)}{R^4}\right] - \gamma - \frac{2}{\pi}\frac{\eta+\xi}{R^4}b_s\tau \tag{A.1}$$

where η is the center of mass of the dislocation pair, ξ is the separation half width, R is the radius of the cylinder, γ is the stacking fault energy, μ is the shear modulus, ν is Poisson's ratio, and τ is the applied torque, negative in the z direction in the sense of a right hand rule. This means that a positive applied torque will tend to drive the dislocations into the cylinder. The three terms coupled with the edge Burgers vector are from the image field of dislocation 1, the image field of dislocation 2 and the stress field of dislocation 2 in an infinite medium. The first three terms with the screw dislocation are the same for the edge dislocation, except they are associated with screw dislocations which both have Burgers vectors b_s. The fourth and fifth terms are associated with the image torque required to make the cylinder torque free. The penultimate term in Eq. (A.1) is the force associated with the stacking fault and the last term is from the applied torque. The force on dislocation 2 may be found in a similar fashion.

From the above elastic solution, we can solve for the cases in which the dislocations are no longer stable inside the cylinder. For the dislocations to be stable in the wire we require $\partial E/\partial\eta = \partial E/\partial\xi = 0$ with $(\partial^2 E/\partial\eta^2)\partial E^2/\partial\xi^2 - (\partial E^2/\partial\xi\partial\eta)^2 > 0$ and $\partial^2 E/\partial\eta^2 > 0$. These quantities can be found by noting that $f_\eta \equiv -\partial E/\partial\eta = f_x^1 + f_x^2$ and $f_\xi \equiv -\partial E/\partial\xi = f_x^1 - f_x^2$. From analyzing the stability of the dislocation pair, one finds that the only stable equilibrium position is when the center of mass is at the center of the wire. There are two other possible equilibrium positions, but they are unstable with respect to perturbations in η.

A negative applied torque may destabilize the dislocation pair. If the dislocation pair sits at the center, then a negative applied torque can either pull the partial dislocations our separately, leaving a stacking fault, or make the dislocation dipole unstable with respect to perturbations of its center of mass. Which path the dislocations take depends on which one has a lower critical torque. If the center of mass is at $\eta = 0$ it can be shown that $\partial E^2/\partial\xi\partial\eta = 0$. The loss of stability of the dislocations reduces to the conditions that $\partial^2 E/\partial\eta^2 = 0$ or $\partial E^2/\partial\xi^2 = 0$ and $\partial E/\partial\eta = \partial E/\partial\xi = 0$. Numerical solutions to these equations show that the critical torque is always lower when $\partial^2 E/\partial\eta^2 = 0$, which means the dislocation pair will always tend to leave together rather than be pulled apart. This makes sense since if the two partials are pulled apart they will leave behind a stacking fault which will have a higher energy that a defect free wire. A positive applied torque will only further stabilize the center position and push the partials in closer.

Appendix B. Critical torque derivation for a Y junction

The change in energy and the work done on a Y junction is zero to first order, which confirms that the structure is in static equilibrium. Therefore, to investigate the stability of the network and establish a critical torque, the configuration must be analyzed to second order in δy. The change in line length of the vertical segment is $\delta L_1 = \delta y$ to second order since it exactly changes length δy in the perturbation. The length change of other two arms are

$$\delta L_2 = \delta L_3 = -\frac{1}{\sqrt{3}}\delta h - \frac{(\delta h)^2}{2R} \tag{B.1}$$

where $\delta h = (\sqrt{3}/2)\delta y$. Thus, the total change in length is

$$\delta L_{\text{tot}} = -\frac{(\delta h)^2}{R} \tag{B.2}$$

Using the line tension approximation and an energy per unit length of $E = (\mu b^2/4\pi)\log(R/b)$ the change in energy is

$$\delta E = -\frac{\mu b^2(\delta h)^2}{4\pi R}\log\left(\frac{R}{b}\right) \tag{B.3}$$

which says that the junction is in an unstable equilibrium if no torque is applied.

The work can be computed from $W = \int_A \sigma_{ij} b_j n_i \, dA$. This integral can be evaluated using cylindrical coordinates as

$$\delta W = -2\int_0^R r \int_0^{(\delta h)/r} \sigma_{\theta z} b \sin\theta \, d\theta \, dr = -2\int_0^R r \int_0^{\delta h/r} \frac{\tau r}{J} b\theta \, d\theta \, dr = -\frac{\tau b R}{J}(\delta h)^2 \tag{B.4}$$

The integral is carried out from $r=0$ to R. This is again an approximation which can be corrected by removing the integral from $r=0$ to $\delta h/2$ and replacing it with a more correct form, where θ would have constant limits of integration from 0 to $\pi/3$. However, this correction is of order $(\delta h)^3$, so it is inconsequential for this derivation.

The critical torque can now be obtained by equating the work, Eq. (B.4), to the change in energy, Eq. (B.3)

$$\tau_c = \frac{J\mu b}{4\pi R^2} \log\left(\frac{R}{b}\right) \tag{B.5}$$

and noting that the polar moment of inertia is $J = (\pi/2)R^4$

$$\tau_c = \frac{R^2 \mu b}{8} \log\left(\frac{R}{b}\right) \tag{B.6}$$

The critical torque derived here is based on line tension arguments which should give us the correct scaling behavior. The exact expression may need to be modified to account directly for elastic interactions.

References

Arsenlis, A., et al., 2007. Enabling strain hardening simulations with dislocation dynamics. Modelling and Simulation in Materials Science and Engineering 15, 553.

Barnett, D.M., Nix, W.D., Private communication.

Brinckmann, S., Kim, J.-Y., Greer, J.R., 2008. Fundamental differences in mechanical behavior between two types of crystals at the nanoscale. Phys. Rev. Lett. 100, 155502.

Bulatov, V.V., et al., 2004. Scalable line dynamics in paraDiS. Supercomputing 19.

Cai, W., et al., 2004. Massively-parallel dislocation dynamics simulations. Solid Mechanics and Its Applications, vol. 115. Kluwer Academic Publishers, Dordrectht, pp. 1.

Cai, W., Fong, W., Elsen, E., Weinberger, C.R., 2008. Torsion and bending periodic boundary conditions for modelling the intrinsic strength of nanowires. J. Mech. Phys. Solids 56, 32–42.

Csikor, F.F., Motz, C., Weygand, D., Zaiser, M., Zapperi, S., 2007. Dislocation avalanches, strain bursts, and the problem of plastic forming at the micrometer scale. Science 318, 251–254.

Dimiduk, D.M., Woodward, C., LeSar, R., Uchic, M.D., 2006. Scale-free intermittent flow in crystal plasticity. Science 312, 1188–1190.

Eshelby, J.D., 1953. Screw dislocations in thin rods. J. Appl. Phys. 24, 176–179.

Eshelby, J.D., 1979. Boundary problems. Dislocations in Solids, vol. 1. North Holland Publishers, Amsterdam, p. 167.

Fleck, N.A., Hutchinson, J.W., 1993. A phenomenological theory for strain gradient effects in plasticity. J. Mech. Phys. Solids 41, 1825–1857.

Fleck, N.A., Hutchinson, J.W., 1997. Strain gradient plasticity. In: Hutchinson, J.W., Wu, T.Y. (Eds.), Advances in Applied Mechanics, vol. 33; 1997, pp. 296–361.

Fleck, N.A., Muller, G.M., Ashby, M.F., Hutchinson, J.W., 1994. Strain gradient plasticity: theory and experiment. Acta Metall. Mater. 42, 475–487.

Greer, J.R., Oliver, W.C., Nix, W.D., 2005. Size dependence of mechanical properties of gold at the micron scale in the absence of strain gradients. Acta Materialia 52, 1821–1830.

Guzman, M.D., Neubauer, G., Flinn, P., Nix, W., 1993. The role of indentation depth on the measured hardness of materials. Mater. Res. Symp. Proc. 308, 613–618.

Hirth, J., Lothe, J., 1982. Theory of Dislocations, 2nd ed. Wiley, New York.

Kubin, L.P., 2003. Geometrically necessary dislocations and strain-gradient plasticity: a few critical issues. Scripta Mater. 48, 119–125.

McClintock, F.A., Prinz, F., 1983. A model for the evolution of a twist dislocation network. Acta Metall. 31, 827–832.

Mishin, Y., Farkas, D., Mehl, M.J., Papaconstantopoulos, D.A., 1999. Interatomic potentials for monoatomic metals from experimental data and *ab initio* calculations. Phys. Rev. B 59, 3393–3407.

Nix, W., Gao, H., 1998. Indentation size effects in crystalline materials: a law for strain gradient plasticity. J. Mech. Phys. Solids 46, 411–425.

Park, H.S., Zimmerman, J.A., 2005. Modeling inelasticity and failure in gold nanowires. Phys. Rev. B 72, 054106.

Parrinello, M., Rahman, A., 1981. Polymorphic transitions in single crystals: a new molecular dynamics method. J. Appl. Phys. 52, 7182–7190.

Uchic, M., Dimiduk, D., Florando, J., Nix, W., 2004. Sample dimensions influence strength and crystal plasticity. Science 305, 986–989.

Weinberger, C.R., Cai, W., 2007. Computing the image stress in an elastic cylinder. J. Mech. Phys. Solids 55, 2027–2054.

Weinberger, C.R., Cai, W., 2010. Orientation dependent plasticity in metal nanowires under torsion: twist boundary formation and Eshelby twist. Nano Lett. 10, 130–142.

Weinberger, C.R., Aubry, S., Lee, S.-W., Cai, W., 2009. Dislocation dynamics simulations in a cylinder. IOP Conf. Ser. Mater. Sci. Eng. 3, 012007.

Zhu, T., Li, J., Samanta, A., Leach, A., Gall, K., 2008. Temperature and strain-rate dependence of surface dislocation nucleation. Phys. Rev. Lett. 100, 025502.